ChemPubSoc Europe

DOI: 10.1002/open.201600133

Open Access ChemistryOPEN Full Papers

Relationship between Side-Chain Polarity and the Self-Assembly Characteristics of Perylene Diimide Derivatives in Aqueous Solution

Jurgen Schill,[a] Lech-Gustav Milroy,[a] Jody A. M. Lugger,[b] Albertus P. H. J. Schenning,*[c] and Luc Brunsveld*[a]

Perylene-3,4,9,10-tetracarboxylic acid diimides (PDIs) have recently gained considerable interest for water-based biosensing applications. PDIs have been studied intensively in the bulk state, but their physical properties in aqueous solution in interplay with side-chain polarity are, however, poorly understood. Therefore, three perylene diimide based derivatives were synthesized to study the relationship between side-chain polarity and their self-assembly characteristics in water. The polarity of the side chains was found to dictate the size and morphology of the formed aggregates. Side-chain polarity rendered the self-assembly and photophysical properties of the PDIs—both important for imminent water-based applications—and these were revealed to be especially responsive to changes in solvent composition.

1. Introduction

Nanostructures fabricated by the molecular self-assembly of π-conjugated polymers and oligomers have been widely explored for diverse applications.[1–3] Whereas polymers have the advantage of solution processing, the self-assembly of oligomers has gained much interest owing to their defined oligomeric structures as well as their tunability and dynamics in the aggregated states.[4–6] In particular, the self-assembly of chromophoric oligomers holds great promise for applications in optoelectronics,[7–9] polyelectrolytes,[10–12] and sensing[13–15] because of their relevant optical properties. In these fields, an attractive class of chromophores, perylene-3,4,9,10-tetracarboxylic acid diimides (PDIs), has been widely used owing to their ease of synthesis, strong intermolecular π–π interactions, which facilitate the self-assembly process, and their excellent electronic and optical properties.[16–18] Research into PDIs has mainly focused on their use in bulk. For example, the liquid crystalline behavior of this dye resulted in semiconducting[19–21] and temperature-responsive materials.[22,23] Moreover, solvent-free techniques were exploited to shape these dyes into well-defined fibers[24] and to prepare oriented nanoporous silica films.[25] In contrast to advances in bulk processing, the number of studies on PDIs in aqueous solution has been limited by their poor solubility. Recent efforts have been made to improve the aqueous solubility of PDIs by introducing hydrophilic substituents at different positions on the perylene core.[26,27] Intrinsic aggregation of these dyes in water was subsequently suppressed by introducing polar dendron substituents at the imide positions and by controlling dendron generation.[28] Hence, side-chain polarity can influence the physical characteristics of conjugated polymers and oligomers in aqueous solution.[29,30] Stable polymer dots were formed through the introduction of hydrophobic side chains,[31,32] whereas the introduction of polar side chains led to dynamic polymers[33] and vesicle formation by combining both hydrophobic and hydrophilic side chains into amphiphilic polymers.[34,35] Similar results were obtained for π-conjugated oligomers bearing hydrophobic side chains that could self-assemble into nanoparticles,[36,37] of either spherical[38–40] or vesicular[41–43] morphologies, whereas the majority of bola-amphiphilic π-conjugated oligomers were molecularly dissolved.[44,45] Moreover, the performance of electronic devices based on PDIs was shown to depend on side-chain polarity.[46–49] Concomitantly, the importance of PDI side-chain polarity in aqueous environments has been touched upon for the design of functional surfactants for

[a] J. Schill, Dr. L.-G. Milroy, Prof. L. Brunsveld
Laboratory of Chemical Biology
Department of Biomedical Engineering
and Institute of Complex Molecular Systems
Eindhoven University of Technology
P.O. Box 513, 5600 MB Eindhoven (The Netherlands)
E-mail: l.brunsveld@tue.nl

[b] J. A. M. Lugger
Macromolecular and Organic Chemistry
and Institute of Complex Molecular Systems
Eindhoven University of Technology
P.O. Box 513, 5600 MB Eindhoven (The Netherlands)

[c] Prof. A. P. H. J. Schenning
Functional Organic Materials and Devices
and Institute of Complex Molecular Systems
Eindhoven University of Technology
P.O. Box 513, 5600 MB Eindhoven (The Netherlands)
E-mail: a.p.h.j.schenning@tue.nl

Supporting Information and the ORCID identification number(s) for the author(s) of this article can be found under http://dx.doi.org/10.1002/open.201600133.

carbon nanotubes.[50] All of these studies concluded that the stability and dynamics of the PDIs were dependent on side-chain polarity, which is therefore also a key parameter for controlling PDI-based supramolecular systems. Although core-twisted PDIs have been studied to obtain kinetic control over co-self-assembly,[51] the influence of the side-chain polarity of PDI derivatives on their physical properties in aqueous solution has not been investigated. Therefore, in this work we studied three PDI derivatives with systematically altered side chains to shed light on how differences in side-chain polarity correlate to changes in the self-assembly properties of these oligomers. A detailed understanding of the physical properties of PDIs is fundamental to the rational design of PDI derivatives for imminent water-based applications.

2. Results and Discussion

2.1. Molecular Design

Three known PDI derivatives with varying side-chain polarity were chosen for this study to allow for a comparison of our solution data with the reported bulk properties and, thereby, the influence of side-chain polarity on the thermotropic properties of these oligomers.[52] As the introduction of swallow tail substituents at the imide position is typically sufficient to impart solubility and as PDI derivatives bearing these substituents have been studied in bulk, hydrophobic and hydrophilic swallow tails were selected as side chains (Scheme 1). Whereas condensation of perylene-3,4,9,10-tetracarboxylic dianhydride with excess amounts of primary amines generally allows access to symmetrical bisimides in high yields, unsymmetrical derivatives are usually prepared by partial saponification in a strong acidic or basic environment followed by a second condensation reaction.[48,52] The preparation of a statistical mixture of symmetrically and unsymmetrically substituted perylene derivatives by treating the dianhydride with a mixture of primary amines reportedly leads to difficulties with purification.[53] For ease of synthesis, however, here the dianhydride starting material was substituted by **SI-3** and heptyloctylamine in a one-pot fashion to yield a mixture of PDIs **1**–**3**. Fortunately, the three derivatives bearing systematically altered side-chain polarity could be conveniently isolated by silica gel column chromatography in yields of 11, 24, and 22, respectively, with an overall yield of 57%. This straightforward synthetic route thus allowed for satisfactory yields of these different PDI derivatives for further studies into their respective self-assembly properties.

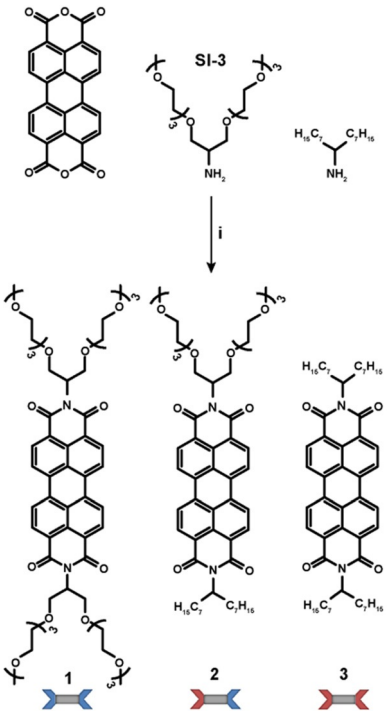

Scheme 1. Synthetic route towards perylene-3,4,9,10-tetracarboxylic acid diimide (PDI) derivatives **1**–**3**. Reagents and conditions: i) imidazole, 180 °C, 16 h, overall yield 57%.[48]

2.2. Thermotropic Behavior

To confirm the bulk properties of the three derivatives, their thermotropic behavior was studied by a combination of differential scanning calorimetry (DSC) and polarized optical microscopy (POM). Moreover, X-ray diffraction (XRD) was measured to study the molecular order in their mesophases. To exclude influences of sample thermal history, the first heating cycle in the DSC measurements was neglected. The phase-transition temperatures observed in the first cooling and second heating cycle are listed in Table 1. The thermograms of PDIs **1**–**3** all show a mesophase upon cooling from the isotropic melt (Figure S1, Supporting Information). XRD measurements revealed that the mesophases exhibit a monotropic hexagonal columnar (Col_h) texture, which was confirmed by polarization microscopy (Figures S2 and S3). Despite the controversy in the literature about the liquid-crystalline behavior of **3**,[54,55] our results are consistent with earlier findings.[47,52] In summary, the liquid-crystalline temperature window of the perylene derivatives could be controlled by means of the side-chain substitution pattern. In addition, the melting point of the liquid-crystalline phase and the clearing temperature revealed to be side-chain dependent, which indicated the impact of the structure–property relationship.

Table 1. Thermotropic behavior of PDIs **1**–**3** as measured by DSC.

PDI	Phase transition[a] 2nd heating cycle	1st cooling cycle
1	Cr (52 °C)→Col_h (120 °C)→I	I (104 °C)→Col_h
2	Cr (59 °C)→Col_h (140 °C)→I	I (133 °C)→Col_h
3	Cr (122 °C)→I	I (115 °C)→Col_h (89 °C)→Cr

[a] Cr = crystalline; Col_h = columnar hexagonal mesophase; I = isotropic.

2.3. Optical Properties and Self-Assembled Structures

The optical properties of the three derivatives were first determined in the molecularly dissolved state by measuring the optical properties in tetrahydrofuran (THF, Figure 1a). In this or-

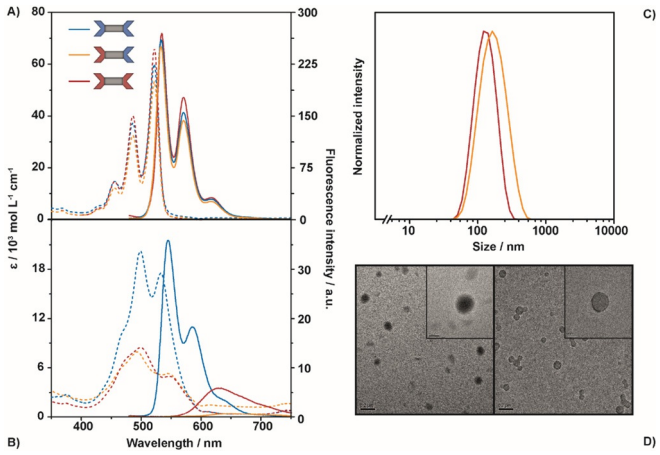

Figure 1. UV/Vis absorption spectra (dashed lines) and corresponding fluorescence spectra (solid lines) of PDI **1**–**3** in a) THF and b) water ($c = 1.5 \times 10^{-5}$ M, $\lambda_{exc} = 455$ nm). c) DLS data of PDI **2** and **3**. d) TEM images of PDI **2** (left) and **3** (right) in water ($c = 1.5 \times 10^{-5}$ M, scale bar: 200 nm); insets show magnified TEM images of the same samples, scale bar: 50 nm.

ganic solvent, the absorption maxima of all three derivatives appear at $\lambda = 522$ nm, along with two higher vibronic transitions located at $\lambda = 486$ and 455 nm, which are characteristic for dissolved PDI chromophores.[18] Additionally, the fluorescence spectra represent a mirror image of the absorption spectra and maintain the vibronic pattern accompanied by well-resolved fine structures. Accordingly, despite the varying imide substituents, the shapes and positions of the absorption and emission spectra are almost identical in their nonaggregated states. The fluorescence quantum yields in organic solution are concomitantly quantitative.

Given the focus of this work on the interplay between self-assembly and side-chain polarity in an aqueous environment, nanosized unimolecular architectures were prepared from PDIs **1**–**3** by means of reprecipitation.[32,56] Rapid injection of a stock solution of each PDI in organic solvent into filter-sterilized demineralized water followed by manual stirring yielded nanosized architectures. These structures were characterized by a range of techniques to study the influence of side-chain hydrophobicity on their physical properties.

In aqueous solution (Figure 1 b), a blueshift in the absorption maxima to $\lambda = 499$ nm is observed. The intensity reversal of the vibronic transitions indicates that the Frank–Condon factor now favors the higher excited vibronic state, which suggests the formation of H-type π–π stacks.[57] Moreover, the distinct drop in overall absorption intensity and clear scattering effects pinpoint the formation of self-assemblies, with PDIs **2** and **3** in similar molecular environments. Owing to a pronounced excitonic coupling between closely stacked oligomers, the fluorescence spectra of PDI **2** and **3** display typical excimer-type broad emission bands with large Stokes shifts that are accompanied by significant drops in the fluorescence quantum yields in aqueous solution (Table S1). This fluorescence quenching process is a well-known feature of H-type perylene diimide stacks in water and has been attributed to aggregation driven by intermolecular π–π interactions.[58] In contrast, PDI **1** still shows a retained vibronic pattern, a moderate Stokes shift, and a relatively high quantum yield. These results suggest that PDI **1** forms weaker π–π interactions than PDIs **2** and **3** and, hence, that smaller aggregates or maybe even partially dissolved molecules in aqueous solution are present, which results in a less pronounced effect on its optical properties (see below).

The hydrodynamic diameters of the formed nanostructures were determined by dynamic light scattering (DLS). Figure 1 c shows the intensity distribution fitted to a spherical model, whereas the directly measured correlograms can be found in Figure S4. These measurements show a strong scattering correlation for PDIs **2** and **3**, though no correlation for PDI **1**, which in the latter case suggests the absence of large aggregates and is in line with the optical properties in water. In contrast, PDIs **2** and **3** measured hydrodynamic diameters of 178 and 123 nm, respectively. Transmission electron microscopy (TEM) analysis of PDIs **2** and **3** drop casted from an aqueous solution indeed reveals regular spherical particles with a monodisperse distribution and an amorphous internal morphology at a low concentration of 1.5×10^{-5} M (Figure 1 d). In addition, the observed particle size in the TEM image is in agreement with the aforementioned DLS data. These results reveal that the side-chain polarity of PDIs **1**–**3** determines their solubility, self-assembly, and, hence, their morphology and optical properties in aqueous solution.

2.4. Self-Assembly Characteristics

Given that nanostructures were formed upon rapid injection of the molecularly dissolved oligomers into water, it is reasonable to assume that these aggregate structures exist in a kinetically trapped state. This assumption was further supported by changing the self-assembly process from reprecipitation to simple dissolution in water, for which fast (PDI **1**, minutes), very slow (PDI **2**, multiple days), or no (PDI **3**) dissolution was observed. The intrinsic binding strength of the PDIs, which is driven by the hydrophobic interactions, was compared by performing absorption measurements in THF-enriched aqueous solutions (Figure S5). The transition from monomers to aggregates occurred at different solvent mixtures depending on the solubility of the oligomers. Intuitively, most hydrophilic PDI **1** showed a transition from monomer to aggregate only in samples with very little THF, whereas most hydrophobic PDI **3** aggregated in highly THF-enriched aqueous solution. Moreover, PDIs **2** and **3** exhibited a sharp transition between the monomeric and aggregate states upon decreasing the THF content, whereas PDI **1** featured a more gradual transition, again highlighting the interplay between side-chain polarity and self-assembly.

With the need for a better understanding of the PDI assembly characteristics towards biomedical applications, the characteristics of PDI **1** were studied in more detail. Temperature-dependent optical measurements of PDI **1** clearly show an increase in both the absorption and fluorescence intensities (Figure 2 a, c). The spectra feature the characteristic signatures of molecularly dissolved oligomers at elevated temperatures.

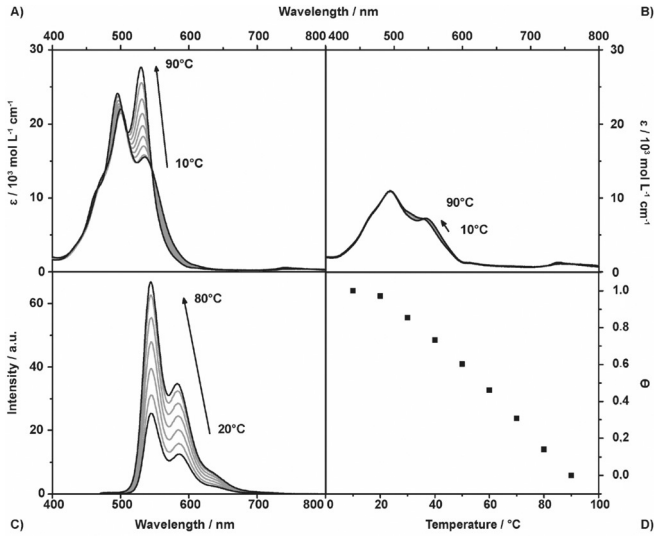

Figure 2. a, b) UV/Vis absorption spectra and c) corresponding fluorescence spectra of PDI derivative **1** (a, c), and **3** (b) in water at different temperatures ($c = 1.5 \times 10^{-5}$ M, $\lambda_{exc} = 455$ nm). Arrows indicate spectral changes upon increasing the temperature in 10 °C intervals. d) Cooling curve for PDI **1**, in which θ is the normalized relative absorbance at $\lambda = 533$ nm ($c = 1.5 \times 10^{-5}$ M).

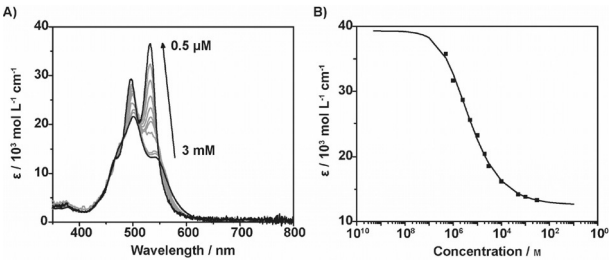

Figure 3. a) Concentration-dependent UV/Vis absorption spectra of PDI **1** in water at 20 °C ($c = 3 \times 10^{-3}$–5×10^{-7} M). The arrow indicates spectral changes upon decreasing the concentration. b) Plot of the extinction coefficient of the monomeric absorbance maximum ($\lambda = 522$ nm) as a function of the concentration of PDI **1** (dots) and fitting curve (line) according to the dimer model.

Hence, a thermodynamic equilibrium for the assembly of PDI **1** can be presumed. Additionally, aggregates of this derivative could not be observed by DLS or TEM, and the monomer-like vibronic pattern observed in the optical measurements of Figure 1 b suggest both small aggregates and molecular dissolved species of PDI **1** in aqueous solution. To elucidate the aggregation mechanism, the absorbance of a typical aggregation band ($\lambda = 533$ nm) was probed as a function of temperature. The resulting cooling curve is characterized by a sigmoidal shape and shows the absence of a critical aggregation temperature (Figure 2 d).[59,60] However, the intrinsic binding constants in aqueous solution are too high to switch the system completely to monomerically dissolved oligomers purely by elevating the temperature, and thus, the melting temperature and concomitant binding constants could not be determined from these measurements.

In contrast to PDI **1**, no significant change in absorption or fluorescence was observed in the temperature-dependent optical measurements of PDIs **2** and **3**, which suggests an extremely high intrinsic binding constant between these perylene derivatives as a result of hydrophobic interactions (Figures 2 b and S6).

To understand the formation of the aggregates of PDI **1** in more detail, concentration-dependent UV/Vis absorption measurements were performed in water. A gradual decrease in the absorption maxima accompanied by a small bathochromic shift was observed, showing a transition from monomeric oligomers to aggregated species upon increasing the concentration (Figure 3 a). A similar transition from monomer to aggregates was also observed by increasing the hydrophobic effect in THF/H_2O mixtures (Figure S5 a). The corresponding plot of the extinction coefficient (ε) versus the concentration of PDI **1** could subsequently be fitted to the dimer model (Figure 3 b).[61] Although the strong aggregation properties of PDI **1** necessitates measuring at low concentrations with resulting low absorption intensity, the intrinsic binding constant of PDI **1** was determined to be 2.2×10^5 M^{-1} in water. The resulting degree of aggregation (α_{agg}) was calculated, and it revealed that the transition from monomeric ($\alpha_{agg} \approx 0$) to aggregated species ($\alpha_{agg} \approx 1$) covers a large concentration range (Figure S7). These findings suggest that ethylene glycol functionalized PDI **1** shows only a weak excitonic coupling in its aggregated state owing to enhanced solubility in polar solvents. In addition, a prohibited longitudinal growth was observed, possibly by steric hindrance or back folding of the side chains and, hence, the formation of only small aggregates.

To further corroborate the confined aggregate size of PDI **1** in aqueous solution, diffusion ordered spectroscopy (DOSY) NMR spectroscopy experiments were conducted (Figure S8). Analysis of the DOSY spectra revealed translational diffusion coefficients of 1.006×10^{-9} and 1.096×10^{-10} $m^2 s^{-1}$ in chloroform and water at room temperature, respectively. Considering the Stokes–Einstein equation, the hydrodynamic radius could be determined (see the Experimental Section). Despite the elongated nature of the aggregates over the assumed spherical morphology in this equation, hydrodynamic radii of 4.0 and 22.4 Å were derived, respectively, which suggests that PDI **1** forms smaller aggregates than PDIs **2** and **3**. To show the dynamic nature of the aggregates of PDI **1** in water, DOSY measurements at elevated temperatures were performed (Figure S8). The diffusion coefficients and, hence, the derived hydrodynamic radii of the aggregates show a linear inverse relationship with temperature and a gradual disassembly process upon increasing the temperature. These results are also consistent with the aforementioned absorption measurements (Figure S9).

3. Conclusions

We have reported the synthesis of three perylene diimide derivatives, each prepared in a one-pot fashion and with each derivative bearing imide substituents with systematically altered side-chain polarity, which is the main factor controlling assembly and dynamics. Subsequent to the analysis and comparison

of their thermotropic behavior in bulk, the influence of side-chain polarity on their aggregation kinetics in aqueous solution was studied. Whereas decreased side-chain polarity resulted in kinetically trapped structures bearing high intrinsic binding constants owing to hydrophobic interactions favorable over aqueous solubility, the introduction of polar side chains resulted in assemblies with a thermodynamic, responsive nature. Concomitantly, small aggregates were observed in absorption and diffusion ordered spectroscopy measurements, and they are likely to be caused by steric hindrance upon longitudinal growth as well as by the increased solubility of the perylene diimide (PDI) derivative. These findings thus clearly demonstrate that side-chain polarity not only plays a key role in bulk but is similarly important for the self-assembly behavior of perylene derivatives in aqueous solution. The polarity of the substituents on the π-conjugated perylene core was found to dictate the size, morphology, and optical properties of the self-assembled nanosized architectures. We foresee this principle to be of value regarding the molecular design of perylene-based systems for imminent water-based applications.

Experimental Section

General Remarks

All solvents employed were obtained from Biosolve BV and were used without purification unless stated otherwise. The reagents were obtained from Sigma–Aldrich and were used without purification. Analytical thin-layer chromatography (TLC) was performed by using Merck precoated silica gel with the use of ultraviolet light irradiation at $\lambda = 254$ and 365 nm. Manual column chromatography was performed by using Merck 60 Å pore-size silica gel (particle size: 63–200 μm). All the NMR spectroscopy data were recorded with a Bruker Advance-III 400 MHz equipped with a BBFO probe from Bruker (400 MHz for ^{1}H and 100 MHz for ^{13}C). Chemical shifts are reported in parts per million (ppm) referenced to an internal standard of residual proteosolvent [D]chloroform ($\delta = 7.26$ ppm for ^{1}H and $\delta = 77$ ppm for ^{13}C, relative to tetramethylsilane as an internal standard). ^{1}H NMR and ^{13}C NMR signals were assigned with the aid of two-dimensional ^{1}H,^{13}C HSQC and ^{1}H,^{13}C HMBC spectra. Matrix-assisted laser desorption/ionization time-of-flight mass spectrometry (MALDI-TOF-MS) was performed with a PerSeptive Biosystems Voyager-DE Pro spectrometer with a Biospectrometry workstation using 2-[(2*E*)-3-(4-*tert*-butylphenyl)-2-methylprop-2-enylidene]malononitrile (DCTB) and α-cyano-4-hydroxycinnamic acid (CHCA) as matrix materials and methylene chloride as the solvent. For LC–MS, a C18, Jupiter SuC4300A, 150×2.00 mm column was used by using H_2O with 0.1% formic acid (FA) and acetonitrile with 0.1% FA with a gradient of 5 to 100% acetonitrile over 10 min at a a flow rate of 0.2 mL min^{-1}. POM was performed with a Jeneval microscope equipped with crossed polarizers, a Linkam THMS 600 heating stage, and a Polaroid DMC le CCD camera. DSC measurements were performed in hermetic T-zero aluminum sample pans using a TA Instruments Q2000-1037 DSC instrument equipped with a RCS90 cooling accessory. Transition temperatures and enthalpies were typically determined from the first cooling and second heating run by using Universal Analysis 2000 software (TA Instruments, USA) with heating and cooling rates of 10 K min^{-1}. XRD profiles were recorded with a Ganesha lab instrument equipped with a Genix-Cu ultralow divergence source producing X-ray photons with a wavelength of 1.54 Å and a flux of 1×10^8 photons s^{-1}. Diffraction patterns were collected by using a Pilatus 300 K silicon pixel detector with 487×619 pixels of 172 μm^2 placed at a sample to detector distance of 91 mm. Temperature was controlled with a Linkam HFSX350 heating stage and cooling unit. Azimuthal integration of the diffraction patterns was performed by utilizing the SAXSGUI software. The beam center and the *q*-range were calibrated by using silver behenate ($d_{(100)} = 0.1076$ Å^{-1}; 58.39 Å); $d_{(300)}$ was used for calibration. Measurements were performed on bulk samples sealed in 1.0 mm diameter glass capillaries, 0.01 mm wall thickness (Hilgenberg). Dynamic light scattering (DLS) experiments were performed with a Malvern Instruments Limited Zetasizer μV (model: ZMV2000). The incident beam was produced by a HeNe laser operating at $\lambda = 632$ nm. Visualization by TEM was performed by a Technai G2 Sphera by FEI operating at an acceleration voltage of 80 kV. Samples were prepared by drop casting a 1.5×10^{-5} M aqueous PDI solution on a carbon film on a 400 square mesh copper grid and were dried for 1 min.

Synthesis

General procedure for the synthesis of imide-substituted perylene derivatives **1**, **2**, and **3**:[48] Perylene-3,4,9,10-tetracarboxylic dianhydride (100 mg, 255 μmol), heptyloctylamine (58 mg, 255 μmol), and **SI-3** (98 mg, 255 μmol) were added to imidazole (500 mg), and the mixture was stirred at 170 °C for 16 h under an argon atmosphere. Subsequently, the mixture was slowly cooled to room temperature and diluted with EtOH/2 M HCl (1:1). The mixture was stirred for 3 h, filtered, and washed several times with a mixture of EtOH/2 M HCl (1:1) and then with warm water. The residue was dried (vacuum stove) to yield a dark-red material that was purified by column chromatography (silica gel, CH_2Cl_2 + 5% MeOH stepwise gradient) to obtain **1**, **2**, and **3** in an overall yield of 57%. The reported ^{1}H NMR and ^{13}C NMR spectroscopy data are in good agreement with ref. [52].

1: Yield: 31.5 mg, 28.1 μmol (11%). ^{1}H NMR (400 MHz, $CDCl_3$): $\delta =$ 8.75–8.40 (m, 8H, 8Ar), 5.75–5.65 (m, 2H, *N*-CH-OEG), 4.19 (dd, $J =$ 10.6, 7.7 Hz, 4H, 2 αOCH$_2$-OEG), 3.99 (dd, $J = 10.6$, 5.8 Hz, 4H, 2 αOCH$_2$-OEG), 3.75–3.43 (m, 48H, 24 OCH$_2$-OEG), 3.28 ppm (s, 12H, 4 OCH$_3$). ^{13}C NMR (100 MHz, $CDCl_3$): $\delta = 164.00$ (4C, CONR), 134.68, 131.60, 129.69, 126.51, 123.23, 123.02 (20C, C$_{Ar}$), 72.02, 70.68, 70.61, 70.60, 70.49, 69.47 (28C, OCH$_2$-OEG), 59.13 (4C, OCH$_3$), 52.30 ppm (2C, *N*-CH). MS (MALDI-TOF): *m/z*: calcd for $C_{58}H_{78}N_2O_{20}$: 1123.24 [*M*]; found: 1122.55 [*M*]$^-$.

2: Yield: 59.2 mg, 61.2 μmol (24%). ^{1}H NMR (400 MHz, $CDCl_3$): $\delta =$ 8.69–8.45 (m, 8H, 8ArH), 5.75–5.66 (m, 1H, *N*-CH-OEG), 5.24–5.13 (m, 1H, *N*-CH), 4.19 (dd, $J = 10.5$, 7.8 Hz, 2H, αOCH$_2$-OEG), 3.96 (dd, $J = 10.6$, 5.8 Hz, 2H, αOCH$_2$-OEG), 3.76–3.50 (m, 20H, 10 OCH$_2$-OEG), 3.48–3.44 (m, 4H, 2 OCH$_2$-OEG), 3.31 (s, 6H, 2 OCH$_3$), 2.36–2.15 (m, 2H, αCH$_2$), 1.96–1.81 (m, 2H, αCH$_2$), 1.42–1.12 (m, 20H, 10 CH$_2$), 0.80 ppm (t, $J = 6.6$ Hz, 6H, 2 CH$_3$).^{13}C NMR (100 MHz, $CDCl_3$): $\delta =$ 163.95 (4C, CONR), 134.65, 134.44, 131.99, 131.56, 131.26, 129.86, 129.63, 126.46, 126.41, 124.07, 123.48, 123.19, 123.03 (20C, C$_{Ar}$), 72.00, 70.66, 70.61, 70.58, 70.48, 69.44 (14C, OCH$_2$-OEG), 59.11 (2C, OCH$_3$), 54.92 (1C, *N*-CH), 52.26 (1C, *N*-CH-OEG), 32.51, 31.93, 29.65, 29.36, 27.13, 22.74 (12C, CH$_2$), 14.20 ppm (2C, CH$_3$). MS (MALDI-TOF): *m/z*: calcd for $C_{54}H_{74}N_2O_{12}$: 967.19 [*M*]; found: 966.50 [*M*]$^-$.

3: Yield: 45.5 mg, 56.1 μmol (22%). ^{1}H NMR (400 MHz, $CDCl_3$): $\delta =$ 8.67–8.47 (m, 8H, 8ArH), 5.23–5.12 (m, 2H, *N*-CH), 2.31–2.18 (m, 4H, 2 αCH$_2$), 1.93–1.81 (m, 4H, 2 αCH$_2$), 1.39–1.15 (m, 40H, 20 CH$_2$), 0.81 ppm (t, $J = 6.6$ Hz, 12H, 4 CH$_3$). ^{13}C NMR (100 MHz, $CDCl_3$): $\delta =$ 164.60, 163.53 (4C, CONR), 134.38, 131.80, 131.07, 129.56, 126.35, 124.00, 123.28, 122.95 (20C, C$_{Ar}$), 54.89 (2C, *N*-CH), 32.50, 31.93,

29.65, 29.36, 27.14, 22.73 (24C, CH_2), 14.18 ppm (4C, CH_3). MS (MALDI-TOF): *m/z*: calcd for $C_{54}H_{70}N_2O_4$: 811.15[*M*]; found: 810.56 $[M]^-$.

Particle Formation

Nanosized architectures were prepared from unimolecular building blocks by means of reprecipitation. This included rapid injection of 15 μL of a 1×10^{-3} M perylene derivative stock solution dissolved in anhydrous tetrahydrofuran (≥99.9%, inhibitor free) into 1 mL filter-sterilized demineralized water followed by manual stirring to yield a 1.5×10^{-5} M nanoparticle solution.

Optical Measurements

UV/Vis spectra were measured with a Jasco V-650 spectrophotometer equipped with a PerkinElmer PTP-1 Peltier temperature control system. The spectra were measured in quartz cuvettes, and extinction coefficients were calculated from Lambert–Beer's law. Fluorescence spectra were recorded with a Varian Cary Eclipse fluorescence spectrophotometer. Fluorescence quantum yields (Φ) were calculated from the integrated intensity under the emission band (I) using Equation (1), for which OD is the optical density of the solution at the excitation wavelength and n is the refractive index. N,N′-bis(pentylhexyl)perylene-3,4:9,10-teteracarboxylic acid bisimide ($\Phi=0.99$) in methylene dichloride was used as a reference.

$$\Phi = \Phi_r \frac{I}{I_r}\frac{\mathrm{OD}_r}{\mathrm{OD}}\frac{n^2}{n_r^2} \quad (1)$$

DOSY Measurements

DOSY measurements were performed by using a bipolar gradient pulse paired stimulated echo and LED (ledbpgp2s) pulse sequence. The self-diffusion of monodeuterated water (HDO) was used to calibrate the machine to its known diffusion constant of 2.299×10^{-9} $m^2 s^{-1}$ in D_2O at 298 K.[62] The Stokes–Einstein equation for the diffusion of spherical particles [Eq. (2)] was used to calculate the hydrodynamic diameter of the aggregates:

$$D = \frac{K_b T}{6\pi\eta r} \quad (2)$$

in which D is the diffusion coefficient, K_b is Boltzmann's constant, T is the absolute temperature, η is the dynamic viscosity, and r is the radius of the spherical particle.

Acknowledgements

The research was supported by funding from HTSM through STW grant 12859-FluNanoPart and by the Ministry of Education, Culture, and Science (Gravity program 024.001.035). We thank H. Janssen (SymoChem BV) for valuable discussions.

Conflict of Interest

The authors declare no conflict of interest.

Keywords: nanoparticles · oligomers · photophysics · self-assembly · supramolecular chemistry

[1] F. S. Kim, G. Ren, S. A. Jenekhe, *Chem. Mater.* **2011**, *23*, 682–732.
[2] T. Aida, E. W. Meijer, S. I. Stupp, *Science* **2012**, *335*, 813–817.
[3] L. Maggini, D. Bonifazi, *Chem. Soc. Rev.* **2012**, *41*, 211–241.
[4] I. Fischer, A. Kaeser, M. A. M. Peters-Gumbs, A. P. H. J. Schenning, *Chem. Eur. J.* **2013**, *19*, 10928–10934.
[5] J. Schill, A. P. H. J. Schenning, L. Brunsveld, *Macromol. Rapid Commun.* **2015**, *36*, 1306–1321.
[6] E. Krieg, M. M. C. Bastings, P. Besenius, B. Rybtchinski, *Chem. Rev.* **2016**, *116*, 2414–2477.
[7] F. J. M. Hoeben, P. Jonkheijm, E. W. Meijer, A. P. H. J. Schenning, *Chem. Rev.* **2005**, *105*, 1491–1546.
[8] E.-K. Fleischmann, R. Zentel, *Angew. Chem. Int. Ed.* **2013**, *52*, 8810–8827; *Angew. Chem.* **2013**, *125*, 8972–8991.
[9] A. Jain, S. J. George, *Mater. Today* **2015**, *18*, 206–214.
[10] L. An, S. Wang, *Chem. Asian J.* **2009**, *4*, 1196–1206.
[11] G. Feng, D. Ding, B. Liu, *Nanoscale* **2012**, *4*, 6150–6165.
[12] R. R. Costa, J. F. Mano, *Chem. Soc. Rev.* **2014**, *43*, 3453–3479.
[13] S. W. Thomas 3rd, G. D. Joly, T. M. Swager, *Chem. Rev.* **2007**, *107*, 1339–1386.
[14] X. Feng, L. Liu, S. Wang, D. Zhu, *Chem. Soc. Rev.* **2010**, *39*, 2411–2419.
[15] S. Rochat, T. M. Swager, *ACS Appl. Mater. Interfaces* **2013**, *5*, 4488–4502.
[16] F. Würthner, *Chem. Commun.* **2004**, 1564–1579.
[17] T. Weil, T. Vosch, J. Hofkens, K. Peneva, K. Müllen, *Angew. Chem. Int. Ed.* **2010**, *49*, 9068–9093; *Angew. Chem.* **2010**, *122*, 9252–9278.
[18] F. Würthner, C. R. Saha-Möller, B. Fimmel, S. Ogi, P. Leowanawat, D. Schmidt, *Chem. Rev.* **2016**, *116*, 962–1052.
[19] G. De Luca, A. Liscio, G. Battagliarin, L. Chen, L. M. Scolaro, K. Müllen, P. Samorì, V. Palermo, *Chem. Commun.* **2013**, *49*, 4322–4324.
[20] J. A. Quintana, J. M. Villalvilla, A. de la Peña, J. L. Segura, M. A. Díaz-García, *J. Phys. Chem. C* **2014**, *118*, 26577–26583.
[21] D. Dasgupta, A. M. Kendhale, M. G. Debije, J. ter Schiphorst, I. K. Shishmanova, G. Portale, A. P. H. J. Schenning, *ChemistryOpen* **2014**, *3*, 138–141.
[22] J. A. Quintana, J. M. Villalvilla, A. de la Peña, J. L. Segura, M. A. Díaz-García, *J. Phys. Chem. C* **2015**, *119*, 14023–14028.
[23] D. Görl, B. Soberats, S. Herbst, V. Stepanenko, F. Würthner, *Chem. Sci.* **2016**, *7*, 6786–6790.
[24] J. C. Singer, A. Ringk, R. Giesa, H.-W. Schmidt, *Macromol. Mater. Eng.* **2015**, *300*, 259–276.
[25] N. Mizoshita, T. Tani, S. Inagaki, *Chem. Commun.* **2012**, *48*, 10772–10774.
[26] D. Görl, X. Zhang, F. Würthner, *Angew. Chem. Int. Ed.* **2012**, *51*, 6328–6348; *Angew. Chem.* **2012**, *124*, 6434–6455.
[27] M. Sun, K. Müllen, M. Yin, *Chem. Soc. Rev.* **2016**, *45*, 1513–1528.
[28] B. Gao, H. Li, H. Liu, L. Zhang, Q. Bai, X. Ba, *Chem. Commun.* **2011**, *47*, 3894–3896.
[29] C. Wu, D. T. Chiu, *Angew. Chem. Int. Ed.* **2013**, *52*, 3086–3109; *Angew. Chem.* **2013**, *125*, 3164–3190.
[30] A. Kaeser, I. Fischer, R. Abbel, P. Besenius, D. Dasgupta, M. A. J. Gillisen, G. Portale, A. L. Stevens, L. M. Herz, A. P. H. J. Schenning, *ACS Nano* **2013**, *7*, 408–416.
[31] J. Pecher, S. Mecking, *Chem. Rev.* **2010**, *110*, 6260–6279.
[32] D. Tuncel, H. V. Demir, *Nanoscale* **2010**, *2*, 484–494.
[33] C. Zhu, L. Liu, Q. Yang, F. Lv, S. Wang, *Chem. Rev.* **2012**, *112*, 4687–4735.
[34] Y. Mai, A. Eisenberg, *Chem. Soc. Rev.* **2012**, *41*, 5969–5985.
[35] J. Zhang, K. Liu, K. Müllen, M. Yin, *Chem. Commun.* **2015**, *51*, 11541–11555.
[36] H. Zhang, D. Wang, R. Butler, N. L. Campbell, J. Long, B. Tan, D. J. Duncalf, A. J. Foster, A. Hopkinson, D. Taylor, D. Angus, A. I. Cooper, S. P. Rannard, *Nat. Nanotechnol.* **2008**, *3*, 506–511.
[37] C. Vijayakumar, K. Sugiyasu, M. Takeuchi, *Chem. Sci.* **2011**, *2*, 291–294.
[38] L. Zhu, C. Yang, J. Qin, *Chem. Commun.* **2008**, 6303–6305.
[39] M. Kumar, S. J. George, *Nanoscale* **2011**, *3*, 2130–2133.
[40] I. Fischer, K. Petkau-Milroy, Y. L. Dorland, A. P. H. J. Schenning, L. Brunsveld, *Chem. Eur. J.* **2013**, *19*, 16646–16650.

[41] X. Zhang, Z. Chen, F. Würthner, *J. Am. Chem. Soc.* **2007**, *129*, 4886 – 4887.
[42] Y.-X. Xu, G.-T. Wang, X. Zhao, X.-K. Jiang, Z.-T. Li, *Langmuir* **2009**, *25*, 2684 – 2688.
[43] X. Zhang, S. Rehm, M. M. Safont-Sempere, F. Würthner, *Nat. Chem.* **2009**, *1*, 623 – 629.
[44] S. K. Yang, X. Shi, S. Park, S. Doganay, T. Ha, S. C. Zimmerman, *J. Am. Chem. Soc.* **2011**, *133*, 9964 – 9967.
[45] H. Liu, Y. Wang, C. Liu, H. Li, B. Gao, L. Zhang, F. Bo, Q. Bai, X. Ba, *J. Mater. Chem.* **2012**, *22*, 6176 – 6181.
[46] K. Balakrishnan, A. Datar, T. Naddo, J. Huang, R. Oitker, M. Yen, J. Zhao, L. Zang, *J. Am. Chem. Soc.* **2006**, *128*, 7390 – 7398.
[47] F. May, V. Marcon, M. R. Hansen, F. Grozema, D. Andrienko, *J. Mater. Chem.* **2011**, *21*, 9538 – 9545.
[48] R. Kota, R. Samudrala, D. L. Mattern, *J. Org. Chem.* **2012**, *77*, 9641 – 9651.
[49] D. M. Pereira de Oliveira Santos, M. G. Belarmino Cabral, A. Bentaleb, R. Cristiano, H. Gallardo, F. Durola, H. Bock, *Chem. Eur. J.* **2016**, *22*, 7389 – 7393.
[50] F. Ernst, T. Heek, A. Setaro, R. Haag, S. Reich, *J. Phys. Chem. C* **2013**, *117*, 1157 – 1162.
[51] D. Görl, X. Zhang, V. Stepanenko, F. Würthner, *Nat. Commun.* **2015**, *6*, 7009.
[52] A. Wicklein, A. Lang, M. Muth, M. Thelakkat, *J. Am. Chem. Soc.* **2009**, *131*, 14442 – 14453.
[53] H. Kaiser, J. Lindner, H. Langhals, *Chem. Ber.* **1991**, *124*, 529 – 535.
[54] W. Pisula, M. Kastler, D. Wasserfallen, J. W. F. Robertson, F. Nolde, C. Kohl, K. Müllen, *Angew. Chem. Int. Ed.* **2006**, *45*, 819 – 823; *Angew. Chem.* **2006**, *118*, 834 – 838.
[55] M. R. Hansen, R. Graf, S. Sekharan, D. Sebastiani, *J. Am. Chem. Soc.* **2009**, *131*, 5251 – 5256.
[56] H. Kasai, H. S. Nalwa, H. Oikawa, S. Okada, H. Matsuda, N. Minami, A. Kakuta, K. Ono, A. Mukoh, H. Nakanishi, *Jpn. J. Appl. Phys.* **1992**, *31*, L1132 – L1134.
[57] S. Yagai, T. Seki, T. Karatsu, A. Kitamura, F. Würthner, *Angew. Chem. Int. Ed.* **2008**, *47*, 3367 – 3371; *Angew. Chem.* **2008**, *120*, 3415 – 3419.
[58] T. Weil, M. A. Abdalla, C. Jatzke, J. Hengstler, K. Müllen, *Biomacromolecules* **2005**, *6*, 68 – 79.
[59] M. M. J. Smulders, M. M. L. Nieuwenhuizen, T. F. A. de Greef, P. van der Schoot, A. P. H. J. Schenning, E. W. Meijer, *Chem. Eur. J.* **2010**, *16*, 362 – 367.
[60] R. van der Weegen, P. A. Korevaar, P. Voudouris, I. K. Voets, T. F. A. de Greef, J. A. J. M. Vekemans, E. W. Meijer, *Chem. Commun.* **2013**, *49*, 5532 – 5534.
[61] R. B. Martin, *Chem. Rev.* **1996**, *96*, 3043 – 3064.
[62] M. Holz, S. R. Heil, A. Sacco, *Phys. Chem. Chem. Phys.* **2000**, *2*, 4740 – 4742.

Received: October 26, 2016
Revised: January 3, 2017
Published online on January 20, 2017

